Biochemistry and Biophysics Reports 31 (2022) 101298

Contents lists available at ScienceDirect

Biochemistry and Biophysics Reports

journal homepage: www.elsevier.com/locate/bbrep

Dynamic observations of various oligomers in amyloid β isoforms using laboratory diffracted X-ray blinking

Jaewon Chang [a,b,*], Tatsuya Arai [a,b], Masahiro Kuramochi [c], Rena Inamasu [a,b], Zhuoqi Lee [a], Tatsunari Ohkubo [b,d], Kazuhiro Mio [b,d], Yuji C. Sasaki [a,b,**]

[a] Graduate School of Frontier Sciences, The University of Tokyo, 609 Kiban Bldg. Kashiwanoha 5-1-5, Kashiwa, 277-8561, Chiba, Japan
[b] AIST-UTokyo Advanced Operando Measurement Technology Open Innovation Laboratory (OPERANDO-OIL), National Institute of Advanced Industrial Science and Technology (AIST), Kashiwa, 277-0882, Chiba, Japan
[c] Graduate School of Science and Engineering, Ibaraki University, 108 N2 Building 4-12-1 Nakanarusawa, Hitachi, 316-8511, Ibaraki, Japan
[d] Graduate School of Medical Life Science, Yokohama City University, 1-7-29 Suehiro, Tsurumi, Yokohama, 230-0045, Kanagawa, Japan

A B S T R A C T

Acceleration of societal ageing has increased the global incidence of geriatric diseases such as Alzheimer's disease (AD), and the demands for proper diagnosis and monitoring of those diseases are also increasing daily. We utilized diffracted X-ray blinking (DXB) for amyloid β (Aβ) isoforms, which are thought to be closely related to AD, to discriminate among the dynamics of individual particles in early and long-term oligomerisation and aggregation inhibiting environments. Among the various Aβ isoforms, the dynamics of Aβ (1–42), which is known to be the most toxic form, were the slowest (the dynamics were lower by 78% com-pared with short-term incubation), and the dynamics were restored (the dynamics increased by 105% compared with normal aggregation) in an environment that suppressed oligomerisation of Aβ (1–42). It has been confirmed that the use of DXB allows measurements of dynamics related to the functional states of the target molecules.

1. Introduction

Amyloid β (Aβ) isoforms are derived from amyloid β precursor protein via secretase cleavage, and they mainly play individual roles in various target cells; Aβ (1–42) and Aβ (1–40) isoforms composed of 42 and 40 amino acids are concerned with improving astrocytes and promoting neurogenesis, respectively [1]. However, aggregates of Aβ (1–42) and Aβ (1- 40) have high cytotoxicity and are detected in patients with Alzheimer's disease(AD) [2,3].

Thus far, the method for dealing with AD has been focused on Aβ aggregation rather than on quantitative diagnosis and impediment of AD progression [4]. The traditional questionnaire, imaging/measuring (counting) the Aβ isoforms molecules are widely used, however, are not suitable for early diagnosis, quantitative monitoring, or *in vitro* tests. Therefore, the current biochemical methods used to diagnose AD are concentrated on selectively detecting Aβ oligomers in peripheral blood with sensitive antibodies [5]. Nevertheless, detection of novel oligomers requires high sensitivity to target pathogenic Aβ, including multiple Aβ isoforms, various oligomers or fibrils, which cannot be detected. Here, we present another strategy in which a biophysical method using X-rays is used, not selective antibodies and evaluations of dispersion for distinct dynamics for oligomerisation of Aβ. The relationship between protein dynamics and their functional state has been consistently studied. For several proteins, including antigen-antibody reactions, a quantitative relationship between dynamics and 'functional state' has been reported [6,7]. We applied a new time-resolved measurement method, diffracted X-ray blinking (DXB), which monitors more area than other biophysical methods and evaluates the dynamics of Aβ (1–42) and Aβ (1–40) with cytoxicity, and Aβ (1–38) with less cytotoxicity [2,3]. The cytotoxicities of Aβ isoforms rely on the degree of aggregation are related to molecular stiffness; therefore, DXB can measure and evaluate molecular motions or dynamics related to the molecular stiffness of the target Aβ with below-Å resolution. We have shown that the dynamics of Aβ (1–42), Aβ (1–40), and Aβ (1–38) isoforms were slower after 96 h of incubation than those after 18 h of incubation, and the dynamics related to oligomerisation depended on incubation time [8]. By assessing the distribution of individual dynamics, it was revealed that these descending dynamics originated from diminishing faster dynamics. In the case of Aβ (1–42), which has the most cytotoxicity and greatest molecular stiffness, the decrease in dynamics was larger than those of other isoforms. We also used DXB to measure inhibited aggregation derived from the C-terminal domain, where the Aβ (1–42) isoform is mostly affected, and the dynamics of Aβ

* Corresponding author. Graduate School of Frontier Sciences, The University of Tokyo, 609 Kiban Bldg. Kashiwanoha 5-1-5, Kashiwa, 277-8561, Chiba, Japan.
** Corresponding author. Graduate School of Frontier Sciences, The University of Tokyo, 609 Kiban Bldg. Kashiwanoha 5-1-5, Kashiwa, 277-8561, Chiba, Japan.
E-mail address: ggooro@naver.com (J. Chang).

https://doi.org/10.1016/j.bbrep.2022.101298
Received 1 March 2022; Received in revised form 8 June 2022; Accepted 8 June 2022

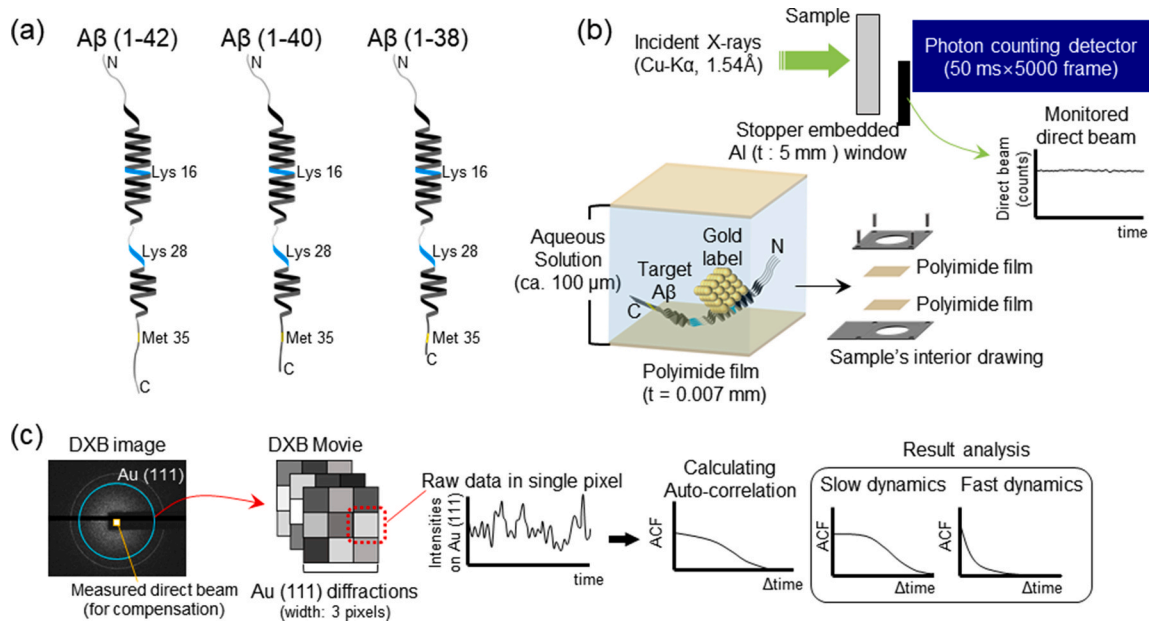

Fig. 1. Sample and DXB measurement. (a) Schematic diagram of Aβ (1–42), Aβ (1–40) and Aβ (1–38). Aβ (1–42) and Aβ (1–40) differ only in C-terminal domain, but the rest of the amino acid sequence is the same. On the other hand, although the structure of Aβ (1–38) was not revealed, it showed similar fibrillogenic behavior to Aβ (1–40), and the arrangement was also closer than Aβ (1–42), so it was referred to Aβ (1–40). (b) Schematic drawing of DXB measurement in this study. Unlike conventional DXB measurement, the direct beam was simultaneously monitored to compensate bias through Al (t: 5 mm) window. (c) ACF analysis in DXB measurement. ACF analysis was performed in pixel by pixel on Au (111).

(1–42) were meaningfully recovered more than those of other isoforms [8,9].

2. Materials and methods

2.1. Oligomerisation and immobilization of Aβ on substrate

We considered Aβ (1–42), Aβ (1–40), and Aβ (1–38) isoforms with few sequence differences in initial reconstitution, as shown in Fig. 1 a, and the only difference among them is the C-terminal domain [10,11]. The DXB measured immobilized and labeled Aβ isoforms on substrate through Lys or Met (shown in Fig. 1 b). DXB measurements are often performed on polyimide films (t = 0.007 mm) with gold deposition [7]. In this study, we titrated Aβ isoforms on gold substrate coated with succinimidyl 3-(2-pyridyldithio)propionate (SPDP). SPDP family is widely used for a cross linker between the gold surface and the primary amine [7]. After the titration, immobilization and oligomerisation were proceeded in an incubator (37°C) for 18 h to measure early oligomer dynamics. More detailed information of samples is shown in S.I. 1, S.I. 2, and S.I. 3.

2.2. Immobilization of stabilized Aβ to substrate

Many studies revealed that Aβ isoforms with high sequence homology are oligomerized by distinct processes. Oligomerisations of the Aβ isoform entered a lull state over 2 days of incubation [8]; therefore, we incubated Aβ isoforms for 4 days in free buffer solution, NOT on a substrate, until they reached a metastable state (shown in S.I. 3 d). It was possible to compare the distinct dynamics of individual Aβ isoforms by early oligomerisation (18 h incubation) and at a stable state (96 h incubation). Stabilized Aβ samples were titrated on a gold substrate coated with SPDP and labeled with gold nanocrystals, while Aβ isoforms for early oligomerisation were manufactured on substrates from scratch (see Section 2. 1).

2.3. Inhibition of the C-terminal domain

We adapted a polyimide film with Pd/Cr vapour deposition to prevent the C-terminal domain from inducing distinct oligomerisation of Aβ (1–42) and Aβ (1–40). We titrated Aβ isoforms on a bare Pd surface and incubated them for 18 h. It was designed that reductive environment and steric hindrance of the C-terminal domain was granted by binding of Met 35 close to the C-terminal domain and Pd (shown in S.I. 3 e) [12].

2.4. Gold labelling

The SPDP cross linker was also used for tethering well-dispersed gold nanocrystals to immobilized Aβ (shown in S.I. 3) [7]. It was presumed that the initial Aβ/substrate binding occurred at Lys 28 with high flexibility, and the subsequent Aβ/gold nanocrystal binding site mainly adapted Lys 16 (shown in Fig. 1 a). After incubation of Aβ on the gold substrate, as described above, the gold nanocrystals coated with SPDP were titrated on the substrate. To eliminate the remaining free Aβ or gold nanocrystals, we gently washed the substrate after Aβ/gold nanocrystal binding (ca. 2 h).

2.5. DXB measurements

A schematic drawing of the sample holder and DXB instrument used in this study is shown in Fig. 1 b. Au (111) diffraction by gold labels was synchronized with the individual Aβ molecule dynamics of the individual target. DXB measurements with various X-ray sources (X-ray tube and synchrotron radiation) allowed discrimination between individual molecular dynamics with high accuracy (<0.01 Å), high speed (25 μs ~0.1 s) and fewer genetic or chemical changes. In this study, the wavelength of incident X-rays was 1.54 Å (Cu Kα, MicroMax-007 HF, RIGAKU), and the scan area was larger (φ70 μm) and brighter (40 kV, 30 mA) than those of other biophysical methods, such as confocal microscopy. Accuracy of the dynamic measurements was sufficient at approximately 0.02 Å for X-ray single molecule dynamics measurements [13]. The diffracted photons were counted by a PILATUS 200 K array (DECTRIS), which was installed 30 mm from the sample holder.

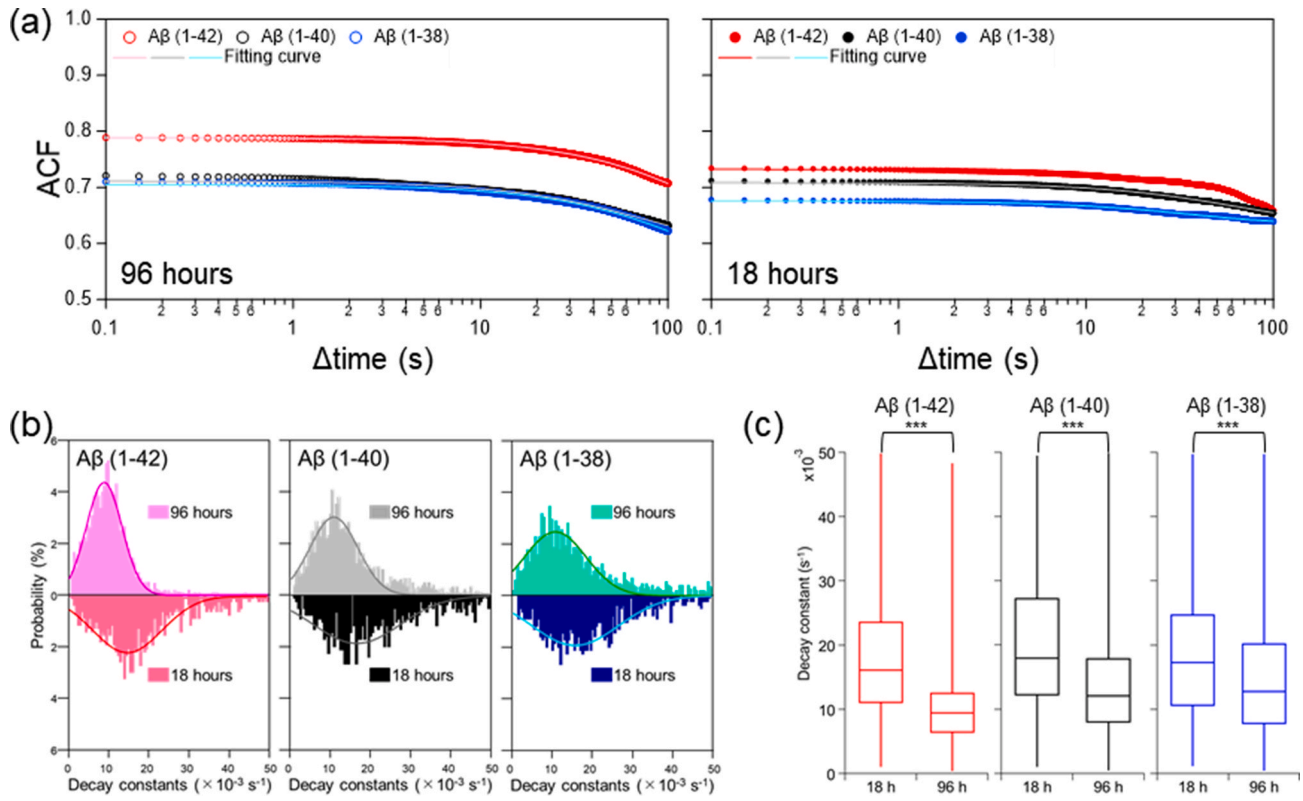

Fig. 2. Aβ isoforms' dynamical changes between long-term (96 h) and short-term (18 h) incubation. (a) Averaged ACF curves of long-term (left) and short-term (right) incubation. (b) Histograms and (c) box plots of decay constants calculated in pixel by pixel. The distributions were compared between long-term and short-term incubation in individual Aβ isoforms. The distributions of all samples were non-parabolic through Shapiro-Wilk normality test, therefore, Wilcoxon rank sum tests were performed: ***p-value < 0.001.

2.6. Calculating and analysing the ACF curve

We monitored the direct beam using an Al window (t = 5 mm) embedded in the stopper while DXB studies were performed (shown in Fig. 1 a and b). The intensity of the direct beam was applied for compensation of Au (111) intensity (shown in Fig. 1 c and S.I. 4). An ACF of the Au (111) intensity for each sample, caused by the DXB measurement, was calculated and applied. The ACF of each sample was calculated over 100 s time intervals (exposure time: 0.05 s, ACF time: 2000 frames) and fitted by a single pixel in Au (111) using the formula below:

$$ACF = \langle I(t) \cdot I(t+T) \rangle / \langle I(t)^2 \rangle = y_0 + A \cdot e^{-\tau \cdot t}$$

where *the brackets is time-averaged values, I(t) is the number of photons, T is the elapsed time, τ is the decay constant, and y_0 and A are fitting parameters.*

The intrinsic decay constant (sec^{-1}), which is the reverse of the lag time (τ^{-1}, sec^1, called the 'time constant') for each fitting curve was regarded as a 'scale of diffusion'. Considering that the first-order exponential function reached 63.2% of the original intensity at the time constant, the fitting curve provided the calculated mobility (Å/s) of each Aβ isoform [6,7,14]. Consequently, a larger decay constant indicated faster dynamics for softer or monomer-like Aβ than the smaller decay constant associated with stiff or oligomerized Aβ. The decay constants obtained through DXB measurements and analyses can be also converted into rotational diffusion constants (diffusivity) through the following equation:

$$D = D_C \cdot \Phi^2 / 4$$

where *D is the rotational Diffusion constant, D_C is the ACF decay constant, Φ represents movements in the time constant* [14] .

However, since the above Φ includes movement of the diffraction spots in all directions, it was not analysed separately for a specific tilting or rotational motion (S.I. 5). Moreover, using a pixel-by-pixel approach (sorted by standard error $< 20\%$, $y_0 > 0$, $A > 0$, and $\tau > 0$), we constructed box plots indicating the median (50%), first (25%), and third (75%) quartiles and the medians for decay constants of individual target Aβ isoforms to estimate dispersion and the fluctuations buried in the ACF of the averaged Au (111) intensity with several noisy or unfitted pixels (shown in Fig. 1 c). We performed Shapiro-Wilk normality test, and the Wilcoxon rank sum tests were performed using the R package [15].

3. Results and discussion

3.1. Shrinked dynamics of stabilized Aβ isoforms in long-term incubation

The diffraction movie for each sample was composed of continuous images from DXB and is usually analysed with ACF curves and regression techniques [6,7,14]. The averaged ACF calculation for DXB on each frame was performed by averaging the intensities of filtered pixels (sorted by ACF calculation and regression analysis for each single pixel (see Section 2. 4) of Au (111) to elucidate the dynamic differences in unified and simplified individual Aβ isoform oligomers (shown in Fig. 2 a). The averaged ACF decay constants(τ^{-1}) of all isoforms in stabilized condition were decreased than early oligomerisation(All averaged ACF decay constants are shown in S.I. 6 a). Furthermore, we analysed histograms for the decay constants consisting of sorted pixels that were more reliable than the averaged ACF and omitted dispersion or diffusion modes (Fig. 2 b). It was determined that the decrease in the faster dynamics and the increase in the slower dynamics constituted a metastable state. The locations of peaks were presumed to be fitted with a single Gaussian. In early oligomerisation, the peak locations of decay constants (τ^{-1}) for Aβ (1–42), Aβ (1–40), and Aβ (1–38) were 1.48×10^{-2}/s, 1.66

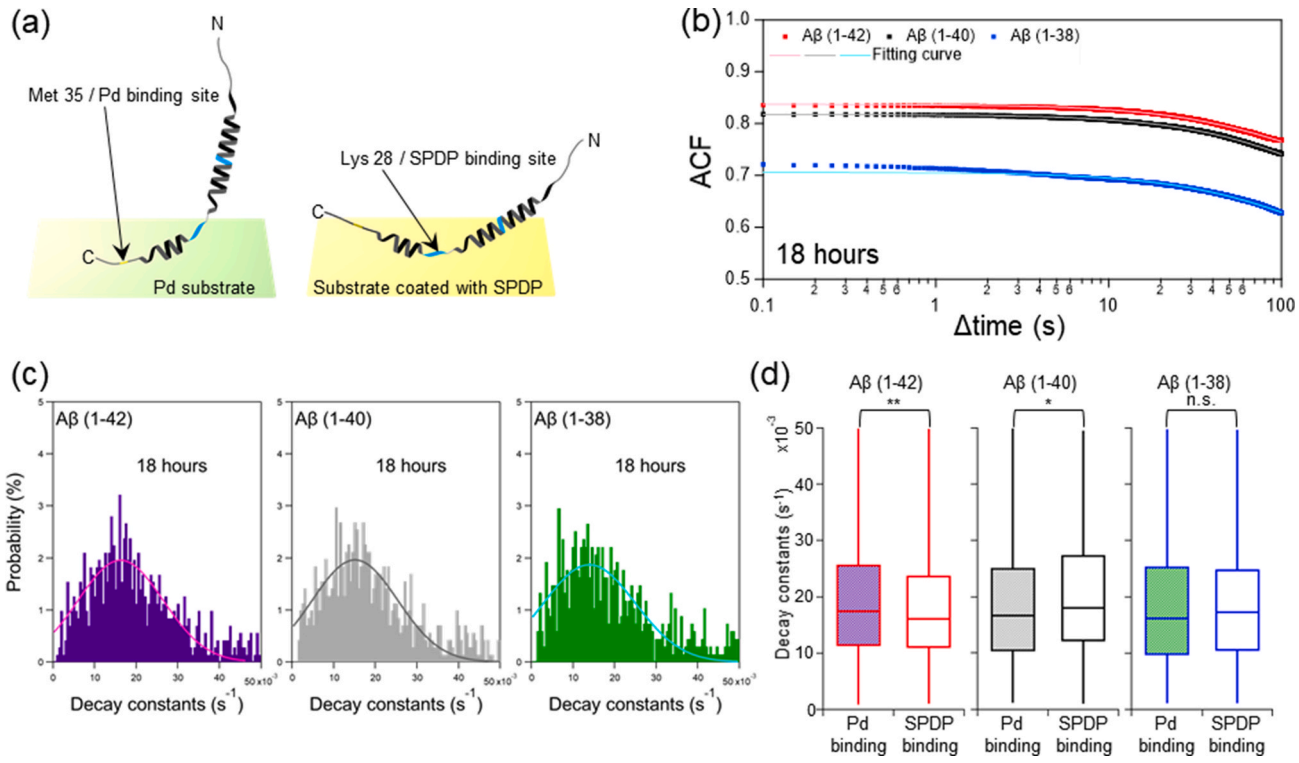

Fig. 3. The dynamics of Aβ isoforms on Pd substrate (incubation time: 18 h) inhibiting oligomerisation through C-terminal domain. (a) Schematic drawing of immobilized Aβ isoforms through Met 35/Pd binding (left). Met 35/Pd binding increase steric hindrance, and ensure the reductive environment which inhibit oligomerisation through C-terminal domain, whereas Au substrate coated with SPDP proceed oligomerisation (right). (b) Averaged ACF curves of Aβ isoforms on Pd substrate. (c) Histograms and (d) box plots of decay constants calculated in pixel by pixel. The distribution was compared between Pd binding and SPDP binding. The distributions of all samples were non-parabolic through Shapiro-Wilk normality test, therefore, Wilcoxon rank sum tests were performed: *p-value<0.05, **p-value<0.01; if not stated: not significant (n.s.).

$\times 10^{-2}$/s, and 1.57 $\times 10^{-2}$/s, respectively (shown in S.I. 6 b). However, in stabilized Aβ isoforms, the peak locations of decay constants of Aβ (1–42), Aβ (1–40), and Aβ (1–38) were 9.05 $\times 10^{-3}$/s, 1.09 $\times 10^{-2}$/s, and 1.09 $\times 10^{-2}$/s, respectively (shown in S.I. 6 b). It was also determined that the trend for dynamics decreased in the order Aβ (1–42), Aβ (1–40), and Aβ (1–38); this is also the decreasing order for toxicity, which is consistent with previous studies [2,8]. The diffusivity (mrad2/s) of each sample was also calculated using the decay constants (see Section 2. 6), the diffusivity of Aβ (1–42) with the highest cytotoxicity were shrinked by 78% (entire diffusivity are shown in S.I. 6 b). Considering the size of Aβ (1–42) oligomer estimated to be 100 nm through transmission electron microscope images (shown in S.I. 2 b), the calculated mobility (Å/s) in early oligomerisation and stabilized state were 0.63 Å/s and 0.49 Å/s, respectively. The double gaussian fittings were tried, it was also reproduced the trend that the dynamics of Aβ (1–42) mostly shrinked (shown in S.I. 6 c). Furthermore, we constructed box plots for sorted pixels of individual Aβ isoforms to investigate previous analyses (shown in Fig. 2 c). Box plots of individual samples were reproduced as histograms and showed that the dynamics of stabilized Aβ isoforms were diminished, and the dynamics of Aβ (1–42) was diminished remarkably (each median of the decay constant is shown in S.I. 6 d). It was also confirmed that the dispersion of dynamics in Aβ (1–42) was decreased mostly, because the width (between 75% and 25%) of box plot was mostly shortened than other isoforms. The distributions of all samples were non-parabolic through Shapiro-Wilk normality test, therefore, Wilcoxon rank sum tests were performed using the R package [15]. All comparisons in short and long-term incubation were statistically significant (shown in S.I. 6 e).

3.2. *Recovered dynamics of Aβ (1–42) in inhibited C-terminal domain*

We performed DXB measurements on the Pd substrate to investigate C-terminal domain induction of different aggregation processes and compared that with data for the Aβ isoforms on the gold substrate coated with SPDP (shown in Fig. 3 a). The averaged ACF decay constants (τ^{-1}) of Aβ (1–42) was recovered than that others (shown in Fig. 3 b). The dynamics of Aβ (1–42) on the Pd substrate for C-terminal inhibitory were faster than that on the gold substrate coated with SPDP (all averaged ACF decay constants are shown in S.I. 7 a). We also analysed the decay constant histograms consisting of sorted pixels and presumed peak locations to determine dispersion or diffusion mode (Fig. 3 c). The peak locations also calculated from single Gaussian fitting were also increased in Aβ (1–42), while others decreased (each location of a decay constant is shown in S.I. 7 b). The diffusivity (mrad2/s) of each sample was also calculated using the decay constants (see Section 2. 6), the diffusivity of Aβ (1–42) with the highest cytotoxicity were increased by 105% (entire diffusivity are shown in S.I. 7 b). The calculated mobility (Å/s) was 0.56 Å/s on Pd substrate (the size of Aβ (1–42) estimated to be 100 nm). Moreover, it was reconfirmed the same trend that the dynamics of Aβ (1–42) on Pd surface recovered than others by the double Gaussian fittings (shown in S.I. 7 c). We also constructed box plots of sorted pixels for individual Aβ isoforms (shown in Fig. 3 d), and the effect of inhibition was verified. The rank for dynamics was reversed in Pd binding versus SPDP binding, and the hardest Aβ (1–42) became softer than the others. Furthermore, it was also shown that the dynamic dispersion of Aβ (1–42) on reductive substrate were recovered remarkably (each median and quartile of the decay constant is shown in S.I. 7 d). Accordingly, it was elucidated that Aβ (1–42) aggregation process aggressively harnessed the oxidative Met 35 and C-terminal domain, including Ile 41 and Ala 42 [9]. The distributions of all Pd binding

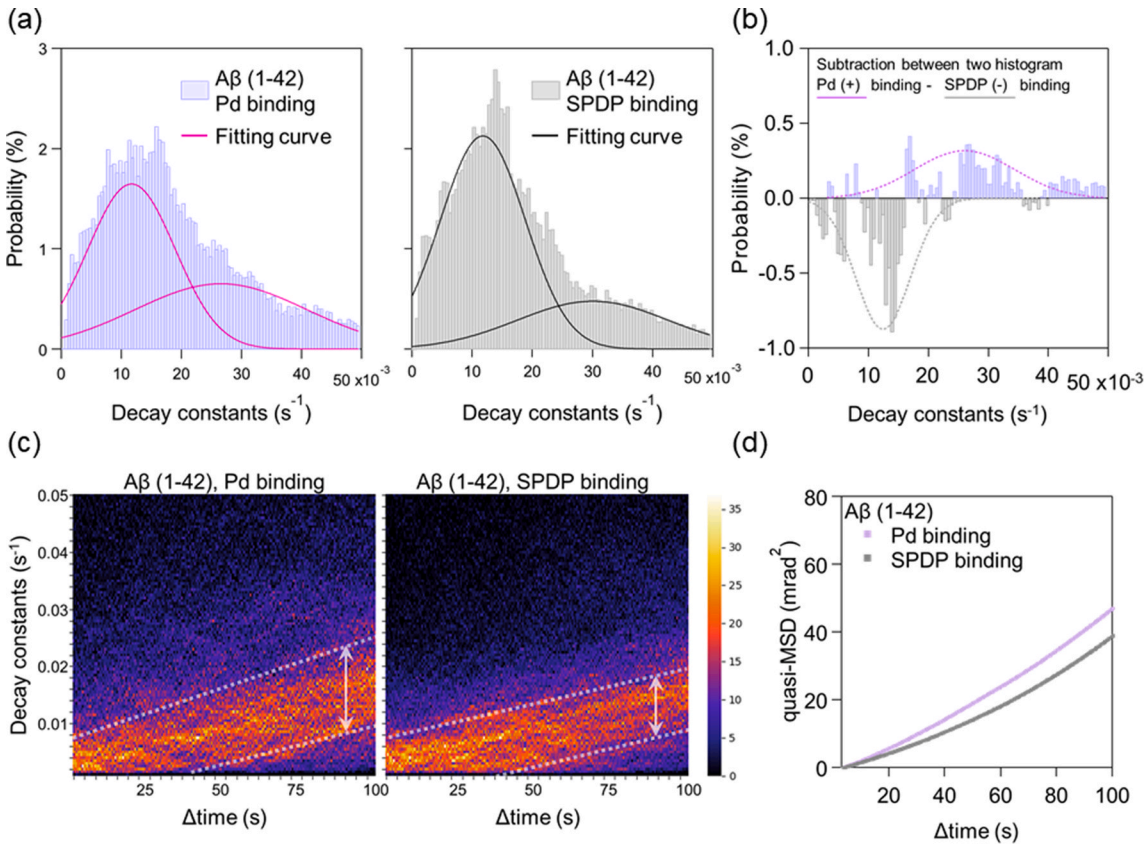

Fig. 4. Analysis of inhibited Aβ (1–42) in cumulative time interval. (a) Time accumulation histograms (cumulative interval: 60 s–100 s, capture interval: 0.5 s) of Pd binding and SPDP binding, and (b) subtract of these histograms. (c) Two-dimensional decay constant heat-map of Pd binding (left) and SPDP binding (right). (d) Quasi-MSD of Pd binding (pink) and SPDP binding (gray) obtained from decay constants/accumulation time plots. (For interpretation of the references to colour in this figure legend, the reader is referred to the Web version of this article.)

samples were also non-parabolic through Shapiro-Wilk normality test, therefore, Wilcoxon rank sum tests were performed using the R package as well [15]. Notably, there was no statistical significance in comparing Aβ (1–38) with other Aβ (1–42) and Aβ (1–40); thus, it was implied that the oligomerisation of Aβ (1–38) had less relation with C-terminal domain compared with that of the other isoform (shown in S.I. 7 e). It was also reproduced through DXB measurement that the aggregation of Aβ (1–42) was most affected by C-terminal domain in the presence of oxidative Met 35 and relatively less in the case of Aβ (1–38) [9].

3.3. Analysis in cumulative time interval

In this study, ACF calculations are mainly performed at 100 s intervals (Δ100s) as described above. Furthermore, time-integration analysis was performed to reveal the recovering dynamics related to inhibition of Met 35/Pd binding and oligomerisation. In the time-integration analysis, ACF calculations were performed every Δ100 s from the 3 s time interval (Δ3 s, 0.05 s exposure time × 60 frame) by increasing the time interval by 0.5 s; accordingly, 195 ACF analyses were finally calculated in individual samples (shown in S.I. 8). In particular, we explored which type of motion was changed in Aβ(1–42), in which inhibition of the C-terminal domain worked effectively and the rank of dynamics were reversed. For Pd binding and SPDP binding of Aβ (1–42), histograms for decay constants from Δ60 s to Δ100 s were drawn, and regression analysis was performed using a double Gaussian. It was found that the proportion of faster dynamics (smaller location) was increased by Pd binding and decreased by SPDP binding by comparing the areas of the individual peaks obtained from regression analyses (shown in Fig. 4 a and S.I. 9). Moreover, the difference between the histograms for Pd binding and SPDP binding were calculated, and it was elucidated that faster dynamics remained for Pd binding and slower dynamics remained for SPDP binding (shown in Fig. 4 b). This was observed in the vicinity of the time interval to be observed (Δ60 s ~ Δ100 s), and it extended to the beginning in the late period. As shown in S.I. 10, to determine the cause of the reversed dynamics ranking, an analysis was conducted in the extended time interval, from the early

(Δ3 s) to the final ACF time (Δ100 s). However, the initial time interval in which the diffraction spots appeared (when diffraction appeared, the intensity was multiplied from '0 counts' to a specific value, which is infinity.) would be better omitted, and it was confirmed that dispersion of the early dynamics was decreased compared with that for latter dynamics. By creating a two-dimensional decay constant heat-map for Δ3 s ~ Δ100 s, it was determined that the dynamics and dispersion of Pd binding were faster than those of SPDP binding (shown in Fig. 4 c and S.I. 11). Furthermore, theoretically, the integral of the rotational diffusion constant for each accumulation time can be represented as a quasi-Mean Square Displacement (quasi-MSD) as shown in below:

$$\mathrm{MSD} = \int \mathrm{D}\ \mathrm{dt}$$

where *D is the rotational Diffusion constant* [16].

Although, this quasi-MSD is a limited quantitative comparison, it was reproduced that

Aβ (1–42) with Pd binding was significantly more active than Aβ (1–42) with SPDP binding at all cumulative times (shown in Fig. 4 d and S.I. 11). Therefore, identify and analyse the dynamic behaviours of molecules, it is more appropriate to review not only a specific time interval but also from a short cumulative time interval.

3.4. Prospect of DXB in diagnosis

Through this study, it was confirmed that the dynamics of Aβ (1–42) were most attenuated by quantitatively distinguishing the initial (18 h incubation) and metastable states (96 h incubation) of Aβ isoforms. In addition, by adapting Met 35/Pd binding, we dynamically discriminated the characteristic oligomerisation of Aβ (1–42) derived from the C-terminal domain without genetic or biological processes. In particular, it was confirmed that the pathological states of Aβ isoforms were detected with distributions for various dynamics, not size comparisons or biochemical methods using antibodies.

Declaration of competing interest

The authors declare that they have no known competing financial interests or personal relationships that could have appeared to influence the work reported in this paper.

Acknowledgments

This work was supported by Ms. R. Kanou. This work was also supported by JSPS KAKENHI Grant Numbers JP20H00324, and by Daikin Industries, Ltd.

Appendix A. Supplementary data

Supplementary data to this article can be found online at https://doi.org/10.1016/j.bbrep.2022.101298.

References

[1] Y. Chen, C. Dong, Aβ40 promotes neuronal cell fate in neural progenitor cells, Cell Death Differ. 16 (3) (2009) 386–394, https://doi.org/10.1038/cdd.2008.94.

[2] Annelies Vandersteen, Marcelo F. Masman, Greet De De Baets, Wim Jonckheere, Kees van der Werf, Siewert J. Marrink, Jef Rozenski, Iryna Benilova, Bart De Strooper, Vinod Subramaniam, Joost Schymkowitz, Frederic Rousseau, Kerensa Broersen, Molecular plasticity regulates oligomerization and cytotoxicity of the multipeptide-length Amyloid-β peptide pool, J. Biol. Chem. 287 (44) (2012) 36732–36743, https://doi.org/10.1074/jbc.M112.394635. https://www.sciencedirect.com/science/article/pii/S0021925820624772.

[3] Maa O. Quartey, Jennifer N.K. Nyarko, Jason M. Maley, Jocelyn R. Barnes, Maria A.C. Bolanos, Ryan M. Heistad, Kaeli J. Knudsen, Paul R. Pennington, Josef Buttigieg, Carlos E. De Carvalho, Scot C. Leary, Matthew P. Parsons, Darrell D. Mousseau, The Aβ(1–38) peptide is a negative regulator of the Aβ(1–42) peptide implicated in Alzheimer disease progression, Sci. Rep. 11 (1) (2021) 431, https://doi.org/10.1038/s41598-020-80164-w. https://www.nature.com/articles/s41598-020-80164-w.

[4] Jeff Sevigny, Ping Chiao, Thierry Bussière, Paul H. Weinreb, Leslie Williams, Marcel Maier, Robert Dunstan, Stephen Salloway, Tianle Chen, Yan Ling, John O'Gorman, Fang Qian, Mahin Arastu, Mingwei Li, Sowmya Chollate, Melanie S. Brennan, Omar Quintero-Monzon, Robert H. Scannevin, H. Moore Arnold, Thomas Engber, Kenneth Rhodes, James Ferrero, Yaming Hang, Alvydas Mikulskis, Jan Grimm, Christoph Hock, Roger M. Nitsch, Alfred Sandrock, The antibody aducanumab reduces Aβ plaques in Alzheimer's disease, Nature 537 (7618) (2016) 50–56, https://doi.org/10.1038/nature19323.

[5] R.B. Mofrad, P. Scheltens, S.Y. Kim, S. Kang, Y.C. Youn, S.S.A. An, T. Jori, van B.N. M. Bart, V. Pieter Jelle, van der F.M. Wiesje, T.E. Charlotte, Plasma amyloid-β oligomerization assay as a pre-screening test for amyloid status, Alzheim. Res. Ther. 13 (1) (2021) 133, https://doi.org/10.1186/s13195-021-00873-w.

[6] Kazuhiro Mio, Masaki Ishihara, Shoko Fujimura, Daisuke Sasaki, Shunsuke Nozawa, Kohei Ichiyanagi, Ryo Fukaya, Shin-Ichi Adachi, Masahiro Kuramochi, Hiroshi Sekiguchi, Tai Kubo, Yuji C. Sasaki, X-ray-based living-cell motion analysis of individual serotonin receptors, Biochem. Biophys. Res. Commun. 529 (2) (2020) 306–313, https://doi.org/10.1016/j.bbrc.2020.05.200.

[7] Jaewon Chang, Yonugseok Baek, Injee Lee, Hiroshi Sekiguchi, Kouhei Ichiyanagi, Kazuhiro Mio, Shunsuke Nozawa, Ryo Fukaya, Shin-ichi Adachi, Masahiro Kuramochi, Yuji C. Sasaki, Diffracted X-ray blinking measurements of interleukin 15 receptors in the inner/outer membrane of living NK cells, Biochem. Biophys. Res. Commun. 556 (2021) 53–58. https://www.sciencedirect.com/science/article/pii/S0006291X21005507.

[8] Peter Niraj Nirmalraj, Jonathan List, Shayon Battacharya, Geoffrey Howe, Liang Xu, Damien Thompson, Michael Mayer, Complete aggregation pathway of amyloid β (1-40) and (1-42) resolved on an atomically clean interface, eaaz6014, Sci. Adv. 6 (15) (2020), https://doi.org/10.1126/sciadv.aaz6014, https://www.science.org/doi/10.1126/sciadv.aaz6014.

[9] Kazuma Murakami, Kazuhiro Irie, Hajime Ohigashi, Hideyuki Hara, Masaya Nagao, Takahiko Shimizu, Takuji Shirasawa, Formation and stabilization model of the 42-mer Aβ radical: Implications for the long-lasting oxidative stress in Alzheimer's disease, J. Am. Chem. Soc. 127 (43) (2005) 15168–15174, https://doi.org/10.1021/ja054041c.

[10] Orlando Crescenzi, Simona Tomaselli, Remo Guerrini, Severo Salvadori, Anna M. D'Ursi, Piero Andrea Temussi, Delia Picone, Solution structure of the Alzheimer amyloid β-peptide (1-42) in an apolar microenvironment: Similarity with a virus fusion domain, Eur. J. Biochem. 269 (22) (2002) 5642–5648, https://doi.org/10.1046/j.1432-1033.2002.03271.x.

[11] Murray Coles, Wendy Bicknell, Andrew A. Watson, David P. Fairlie, David J. Craik, Solution Structure of Amyloid-Peptide(1-40) in a Water-Micelle Environment. Is the Membrane-Spanning Domain Where We Think It Is? Biochemistry 37 (31) (1998) 11064–11077, https://doi.org/10.1021/bi972979f. https://pubs.acs.org/doi/10.1021/bi972979f.

[12] Robert L. Johnson, Thomas J. Schwartz, James A. Dumesic, Klaus Schmidt-Rohr, Methionine bound to Pd/γ-Al2O3 catalysts studied by solid-state 13C NMR, Solid State Nucl. Magn. Reson. 72 (2015) 64–72, https://doi.org/10.1016/j.ssnmr.2015.09.007.

[13] Ahmet Yildiz, Paul R. Selvin, Fluorescence imaging with one nanometer accuracy: Application to molecular motors, Accounts Chem. Res. 38 (7) (2005) 574–582, https://doi.org/10.1021/ar040136s.

[14] Masahiro Kuramochi, Hiroki Omata, Masaki Ishihara, Sander Hanslin, Masaichiro Mizumaki, Naomi Kawamura, Hitoshi Osawa, Motohiro Suzuki, Kazuhiro Mio, Hiroshi Sekiguchi, Yuji C. Sasaki, Tilting and rotational motions of silver halide crystal with diffracted X-ray blinking, Sci. Rep. 11 (1) (2021) 4097, https://doi.org/10.1038/s41598-021-83320-y. https://www.nature.com/articles/s41598-021-83320-y.

[15] Torsten Hothorn, Kurt Hornik, Wirtschaftsuniversität Wien, Mark A Van De Wiel, Achim Zeileis, Implementing a Class of Permutation Tests: The coin Package, J. Stat. Software 28 (8) (2008) 1–23, https://doi.org/10.18637/jss.v028.i08. https://www.jstatsoft.org/article/view/v028i08.

[16] R. Balescu, Hai Da Wang, J.H. Misguich, Langevin equation versus kinetic equation: Subdiffusive behavior of charged particles in a stochastic magnetic field, Phys. Plasmas 1 (12) (1994) 3826–3842, https://doi.org/10.1063/1.870855.